Journal of Crystal Growth 652 (2025) 128045

Contents lists available at ScienceDirect

Journal of Crystal Growth

journal homepage: www.elsevier.com/locate/jcrysgro

Broadband InGaAsP/InP NIR LEDs based on multiple photon-recycling photoluminescent layers

Zoltán Szabó *, Barbara Beiler, Zsófia Baji

HUN-REN Centre for Energy Research, 1121 Konkoly Thege Str. 29-33, Budapest, Hungary

ARTICLE INFO

Communicated by Knut Deppert

Keywords:
NIR
LED
NIRLED
Near infrared
Light emitting diode
InGaAsP
LPE

ABSTRACT

Infrared spectroscopy is a very popular measurement technique presently, especially in healthcare, agriculture, and food industry. NIR LEDs have high efficiencies, but narrow wavelengths, therefore they are suitable for measurements at a certain wavelength. GaInAsP/InP is an ideal material system for the fabrication of double heterostructure LED devices with tuneable emission wavelengths. The present study addresses the need when a broader emission-peak is preferred for spectroscopic applications. An LED structure is covered by photoluminescent layers grown epitaxially by liquid phase epitaxy. The primary light of the active layer excites the further layers which emit photoluminescent radiation. The partly transmitted primary and the secondary lights together result in a broader spectrum. This work presents NIR LEDs with wide emission spectra which cover the entire NIR range based on multiple photon-recycling photoluminescent layers. This type of NIR light source could replace the incandescent light sources on account of their small dimensions, high efficiency, and low power consumption, which is critical in small, handheld NIR spectroscopy devices.

1. Introduction

Near-infrared (NIR) light in the range of 950–1700 nm is invisible to the human eye, less likely to be scattered by dust and other particles in the air or media making it ideal for applications such as chemical analysis, medical imaging and remote sensing. NIR spectroscopy is a fast, non-destructive [1].

NIR spectra of organic materials contain highly valuable information about the quality and content based on the overtones and combination of vibrational modes involving C–H, O–H and N–H chemical bonds. Some applications based on absorbance at 2–3 specific wavelengths are used in everyday industrial workflows such as moisture [2], protein, fat or alcohol content measurements [3,4], plastic separations etc [5]. Near IR light is also optimal for the non-invasive examination of the state of human tissue, bioimaging, or disease diagnosis [6]. NIR infrared light can be divided into two bands, NIR-I (700–900 nm), and NIR-II (900–1700 nm), both of which are used in biosensing and in vitro non-destructive imaging, but the latter has a deeper penetration depth in biological tissues. Nowadays, few miniature spectrometers are already in the market (Texas instr. DLP NIRScan Nano, Vavi micronir 1700, Si-ware systems NIRQuest 2, Spectral engines NIRScan One, etc.) in some cases with already made crowdsourced AI systems for measurement evaluation and building a central cloud database. These products typically contain miniature incandescent light sources or 4–8 discrete LEDs covering the whole spectral range.

In all these applications, the use of LEDs compared to other light sources presents many advantages: they have very small dimensions therefore they act as point light sources, while their power consumption is very low, therefore they are optimal for low-cost miniature devices as well as light sources with arbitrary shapes. One disadvantage of LED sources, however, is that they have a narrow emission spectrum (around or under 50 nm), which can be widened with the use of a phosphorous material which converts a certain ratio of the emitted light to another wavelength [7,8,9,10]. The research and development of new phosphorus materials has been very popular in the past decade. Broad emission LEDs in the visible spectrum are already widespread. On the one hand, there is a greater demand for this range, and on the other hand, as the human eye sensitivity is rather low with only three types of colour-sensitive receptors, the use of three distinct colours can already be experienced as broad spectrum, by humans. However, broadband IR or near IR LEDs are far less developed, but a great effort is present to develop phosphor converted LEDs that combine a blue LED with a well matched broad band NIR phosphor ($Ca_2LuZr_2Al_3O_{12}:Cr^{3+}$ [7], $LiScGe_2O_6:Cr^{3+}$ [8], $La_3Ga_5GeO_{14}:Cr^{3+}$ [9] or $Mg_3Ga_2GeO_8:Cr^{3+}$ [10]), but

* Corresponding author.
E-mail address: szabo.zoltan@ek.hun-ren.hu (Z. Szabó).

https://doi.org/10.1016/j.jcrysgro.2024.128045
Received 16 September 2024; Received in revised form 29 November 2024; Accepted 10 December 2024
Available online 12 December 2024

the optimal solution has not yet been found. Other solutions are also examined such as the one with multiple quantum wells with different centre wavelengths in a transverse junction [11] or the other dual LED grown in one step separated afterwards with etching and selective doping [12].

The quaternary material system of $Ga_xIn_{1-x}As_yP_{1-y}$ is very advantageous, because the band gaps of the solid solutions can be altered by varying the composition of the four components, while keeping their ratio appropriate to preserving the crystalline structure and maintaining perfect epitaxy with the InP substrate [13]. This material family can be used both for sensing photodiodes and for LEDs. The emission spectrum of these LEDs is also very thin, and for broadband applications, it needs to be widened.

Our previous work [14] reports the preparation of broad-spectrum LED heterostructures, where two light emitting layers were integrated in one device structure in order to combine two wavelengths to obtain a broader emission spectrum. In this case one quaternary LED structure served as an electrically excited light source, while the other was optically excited as it absorbed the light of the first and re-emitted another wavelength. This procedure can be further tuned so that the emission peaks match the relevant wavelengths of experimentally relevant structures, in this case, they were set to fit the absorption bands of C–H bonds for the purpose of sensing devices. The resulting spectrum is similar to the phosphor-based broadband emitters, but due to the epitaxial growth and the lattice matching, better efficiency is achieved in a single manufacturing step.

Due to the advantages of the InGaAsP quaternary system, the further improvement of this idea is possible, by adding more optically excited structures. The InGaAsP layers partly absorb and then re-emit the primary photons. The engineering the peaks by tuning the composition and thickness of the layers to homogenously cover the NIR spectrum. This paper reports the development of NIR LEDs with broad emission spectrum using multiple secondary photoluminescent layers (PLs). The PLs convert a part of the primary electroluminescent light to longer wavelengths, resulting in a broad emission spectrum. The optimal thickness (about 1–1.5 um) of the active emitting layer to maximize its output power was calculated and experimentally tested. [15,16,17].

2. Experimental details

Standard double heterojunction (DHJ) InGaAsP/InP layer structures consist of an n-type InP layer, an intrinsic quaternary layer (as the active EL emitter), a p-type InP layer and a p^+-doped InP contact layer. The composition of the $In_{1-x}Ga_xAs_yP_{1-x}$ quaternary layer is tailored to the desired final emission wavelength through the precise setting of the bandgap.

In a multiwavelength LED structure, additional photoluminescent layers are inserted in the layer structure. In practice, this means that the photoluminescent layers are first grown on the InP substrate, and this is followed by the preparation of the heterojunction, each separated by InP spacers.

An additional anti-meltback layer may be necessary after the quaternary layers with a high Ga content (typically above 25 %) to prevent the dissolution of previously grown layers during the growth of subsequent layers. When a significant concentration difference exists between two layers, the already grown layer with higher concentration can dissolve into the lower concentration melt during the subsequent growth. To prevent this dissolution and maintain the integrity of the layer structure, an anti-meltback layer is inserted between the two layers with an intermediate concentration.

In this layer configuration, as it is intended as an inverted LED structure, the electrically excited primary light directly propagates through the photoluminescent layers generating the secondary wavelengths. The layer structure and the preparation sequence are shown in Fig. 1.

Liquid phase epitaxy (LPE) is a very versatile technique for growing

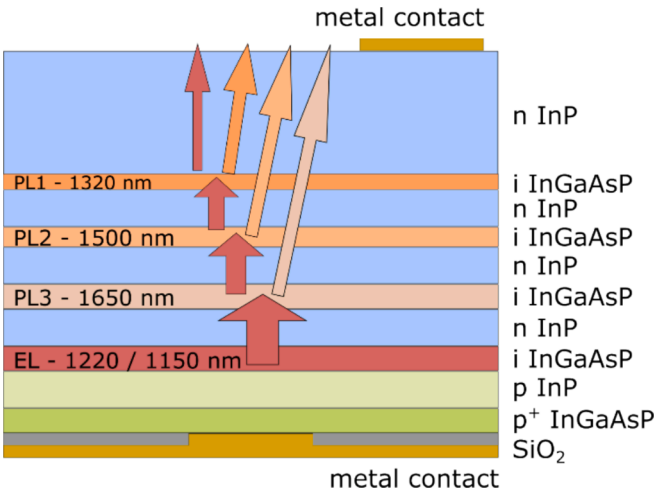

Fig. 1. Schematic diagram of the layer structure.

thick, epitaxial semiconductor layers with various compositions on crystalline substrates. This method involves dissolving the desired elements in a high-temperature molten solution, which is then brought into contact with the substrate. As the solution cools, the dissolved elements supersaturate and precipitate onto the substrate, forming a single-crystal layer. The composition of the grown layers can be simply adjusted by weighing the small amount of materials into the melt, however, other critical parameters, such as the growth temperature, cooling rate, the supersaturation of the melts and the growth time must to be controlled precisely.

The InP, InGaAs ternary and InGaAsP quaternary layers were grown in a custom build LPE system shown in Fig. 2. The quartz reactor tube was heated to 580–650 °C in H_2 atmosphere by a single-zone furnace. The layers were grown on a lattice matched (1 0 0) oriented n-type InP substrate. The graphite sliding boat contained 7 bins for the indium melts and a sunk nest for the substrate. The slider was controlled by a programmable linear actuator synchronized to the temperature controller. The single-phase melts are in relatively high supersaturation during the layer growth. The right amount of InP, GaAs and InAs components were precisely measured, dissolved in the indium solvents, and homogenised at 670 °C before the growth step. The composition of the melts was calculated based on the phase diagram of Kuphal[18] slightly modified based on our large amount of previous experimental data carried out on our LPE system. The n-type and p-type dopants (1–2 × $10^{18}/cm^3$) of the confinement layers were Sn and Zn.

The band gap of the grown InGaAsP layers is between 0.75 eV (ternary boundary) and 1.35 eV (InP), corresponding to the optical bandgap of 1650 nm and 910 nm in wavelength. Layers with bandgaps between 1300–1500 nm were prepared at higher temperatures (640–650 °C) due to the miscibility gap[18], while the layers with lower than 1300 nm bandgap and the ones with 1650 nm bandgap were grown at lower temperatures (580–600 °C) due to the better stability and lower evaporation rate of the volatile P-content of the melts and lower diffusion of the Zn content.

Due to the high number and the large variety of the layers, two consecutive LPE growth steps had to be carried out in our 7-crucible LPE reactor. It is necessary to keep the epitaxial layer formation and the good crystal quality in the 2nd growth step as well, therefore, the native oxide layer was removed in $HCl:H_2O:H_2O_2$ solution just before the growth.

Four different layer structures were prepared with slightly different layer thicknesses. Sample nr. 1. Has an active electroluminescent (EL) layer with an emitted wavelength of 1220 nm. Samples 2–4 have an emitted wavelength of 1150 nm. The difference in samples 2–4 is the thickness of the photoluminescent layers. This is described in detail in Table 1. and the SEM measured thicknesses are shown in Fig. 4.Table 2.

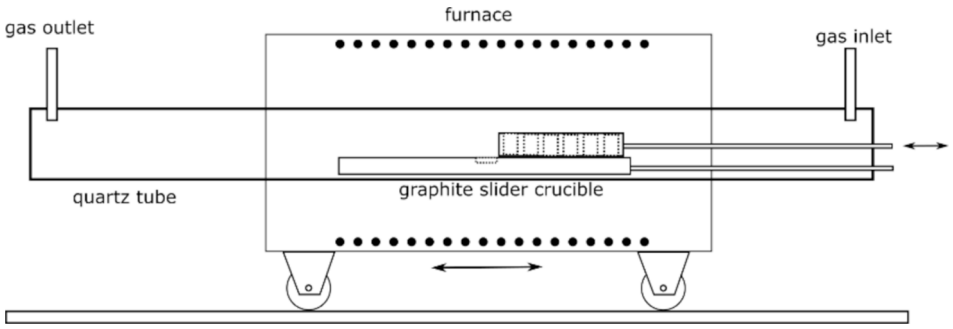

Fig. 2. Schematic of the LPE system.

Table 1
The designed layer structures. Thickness of the PL layers are varied via tuning the growth times or supersaturation.

Layers		designed peak wavelength [nm]	Growth time [s]	ΔT [K]	Designed thickness [μm]
LPE 1	**PL1**	**1320 nm**	**60**	**6**	**1.7**
	spacer		180	8	2.6
	PL2	**1500 nm**	**10**	**4.5–6**	**0.6–0.8**
	anti-meltback	1150 nm	5	7.5	0.4
	spacer		120 + 360	7 / 5.5	2.7
LPE 2	**PL3**	**1650 nm**	**5–10**	**1.3**	**0.1–0.3**
	anti-meltback	1280 nm	3	9.5	0.2
	spacer		120	8	0.8
	active	**1220 / 1150 nm**	**120–180**	**7–8**	**0.8–1**

The wafers were characterized by optical transmittance spectroscopy and photoluminescence spectroscopy right after the 1st and 2nd LPE growth steps. Control Development NIR-256L-1.7 T1 spectrophotometer was used in the range 907–1690 nm, and AvaSpec-NIR512-2.5-HSC-EVO spectrophotometer was used in the range 1340–2500 nm. Light was transmitted along Avantes IR400 400 μm diameter single core fiber optic cables from the light source to the sample, and from the sample to the detector. In the case of the transmittance measurement 6 mm diameter collimator lenses were used at the end of the optical cables. Avantes AvaLight-Hal with ca. 2.5 mW output power was used as a white light source. Photoluminescence map was took using different NIR LEDs as excitation source in the 950–1700 nm range with ca. 1 mW optical power collimated by hemispherical lens. Photoluminescent emissions were collected with a 50 mm inner diameter integrating sphere. Reference intensities were taken through bare InP substrates in similar geometries with every light source. Emission spectra were corrected with a halogen light source as an ideal black body emitter.

The optical band gap of the grown InGaAsP layers were estimated based on the first derivative of the transmittance spectra. The optical band gap was read out from the position of the peak of the derivative spectrum, the height and FWHM of the peaks refer to the thickness and homogeneity of the layers.

LED devices were fabricated from the grown layer structrues. Silicon-oxide was deposited on top of the structures by CVD. Optical lithography with the consecutive wet etching was used to create the required 100 μm openings on the SiO_2 layer for the restricted area bottom contacts (Zn-Au), which were prepared by vacuum evaporation. The back side of the substrate was thinned by a grinding and polishing step followed by the evaporation of the top metal contacts (Sn-Au) through a shadow mask. After this the chips were diced and bonded.

The I-V curves of the LEDs were taken. The emission spectra were measured with the above mentioned equipments. The optical power was measured with a Hamamatsu GaAsP photodiode and the sensitivity was corrected with the emission spectrum. The optical power vs. current was plotted.

3. Results

3.1. Layer structure design

Wide emission spectrum LEDs were prepared by the liquid phase epitaxy of one electroluminescent layer and three epitaxial photoluminescent layers on a (100) sulphur doped InP wafer. The concept is that the three PL layers transform a given ratio of the primary emitted light to different wavelengths and the sum of the four results in a continuous wide spectrum consisting of four peaks.

Once again, it is important to note that the composition of the active EL layer defines the bandgap and through this, the emitted wavelength. The thickness, on the other hand, is set to optimise the emitted intensity: A certain volume of material is required to emit sufficient intensity of light, that is, too thin layers are insufficient. At the same time, too thick layers result in an increased self-absorbance of the emitted light, which is also disadvantageous. An optimum of layer thickness must be experimentally found, although a theoretical approximation and experimentally verified value of 1–1.5 μm is given by ref. [19] in a similar LED structure. The problem of the thickness of the photoluminescent layers is even more complex, as a large volume is required to absorb the exciting light, and to emit the new wavelength, but the self-absorption must also be kept at a low rate. The remaining intensity of λ_1, the primary light after passing through the L thickness of material with α_1 extinction coefficient is:

$$I_{\lambda 1} = I_0 \bullet e^{-\alpha_1 L}$$

If the absorbed intensity is converted into λ_2 wavelength with 100 % efficiency, the additional self-absorption must also be taken into account with an α_1 extinction coefficient. The total converted and emitted λ_2

Table 2
Distribution of the optical output power between the 4 emission wavelengths, the power conversion efficiencies and the approximate total optical power at the active wavelength 1220 nm used in the PL conversion mechanism in Sample 1.

S1	total		active layer1220 nm	PL11320 nm	PL21500 nm	PL31650 nm
P_{opt} **[mW]**	0.461	→	0.035	0.029	0.173	0.224
$\lambda_{exc}/\lambda_{PL}$			1	0.924	0.813	0.74
P_{exc} **[mW]**	0.582	←	0.035	0.031	0.213	0.303

intensity integrated across the whole thickness of the photoluminescent layer is:

$$I_{\lambda 2} = \frac{\alpha_1}{\alpha_1 - \alpha_2}\left[e^{-\alpha_2 L} - e^{-\alpha_1 L}\right]$$

The curve has a maximum intensity value (and conversion efficiency) at:

$$L_{max} = \frac{log(\alpha_1/\alpha_2)}{\alpha_1 - \alpha_2}$$

which is the optimal thickness of the photoluminescent layer, where the PL emission at the secondary wavelength has the maximum value.

In the above equations α_1 is typically higher (5000–10000 cm^{-1}), because λ_1 is lower ($E_{h\nu}$ is higher) than the band gap of the photoluminescent layer. For lower wavelengths, the absorption coefficient is even higher, as it linearly increases with the decreasing wavelength. α_2 is the absorption coefficient of an InGaAsP layer, which increases rapidly below its optical bandgap, its value at the bandgap (self-absorption) is 1000–6000 cm^{-1} [15], λ_2 is right in the middle of the ramp up of the absorbance spectrum (according to the literature [20] and own measurement data. To apply the above equations to the materials in the scope of the present research and the absorption coefficient of these materials, the calculations suggest that the PL layer thicknesses of a few hundred nanometres are optimal, and the photoluminescent layer thickness should be kept below this value, because above this thickness, the overall efficiency decreases. The intensity is accordingly very sensitive to the layer thickness. If the photoluminescent layer is thinner than the optimum, then more primary light is transmitted, on the other hand, if it is too thick, then an excessive loss of the primary wavelength can be experienced. In the case of these multi-photoluminescent layer structures, the ratio of the PL emission and the absorbed excitation can be calculated for the case of the first, second, etc. photoluminescent layers, with specific care that a required intensity of the primary light still be partially transmitted. The resulting spectrum can be optimised by the ratio of the different wavelength lights through the thicknesses of the photoluminescent layers. In the first approach, it is optimal if after the EL layer, which has the lowest wavelength, the photoluminescent layers are ordered from the higher to the lower wavelengths, so that the once reemitted light will not be absorbed again by the following layers, and only the primary light excites secondary photoluminescence. If reflection within the layer structure can be neglected, the emitted intensities can be reliably designed.

The complexity of the layer structure is increased by the presence of the very thin (~300 nm) anti-meltback layers, which increase the absorption. However, the photons absorbed in these layers excite charge carriers, but as the band gaps of these layers are wider than the following photoluminescent films, the excited carriers easily diffuse into the photoluminescent layers and contribute to the light emission there, thus adding to the photoluminescent intensity.

The layer structure is designed to yield wavelengths that ensure a regular coverage of the spectrum. As the peak widths at higher wavelengths widen, this must be taken into account in the design of the position of the peaks. This way the emission peaks should be evenly distributed in the energy domain. The main designs parameters for samples from S1 to S4 are listed in table 1. In practice, the PL1 and PL2 layers are grown in the first step on each substrate, followed by a validation by transmission and photoluminescentce measurements. Based on the transmittance measurements, slight changes in design parameters were implemented into the next sample preparations to adjust the balance between the peaks beloning to the first two PL layers in the first derivative of the transmittance spectra. The preparation parameters of PL1 (1320 nm) were fixed, while the thickness of PL2 was varied with the supersaturation first raised up from 5 °C to 6 °C to get thicker layer, then lowered to 4.5 °C to get a thinner layer. After this optimisation of the PL1 and PL2 films, followed the preparation of the PL3 and the EL layers. To test different configurations, electroluminescent layers with 1220 nm (S1) and 1150 nm (S2-S4) emissions were chosen. The 1150 nm excitation offered an even wider resulting cumulated spectrum. The thickness of the PL3 (1650 nm) layer was slightly adjusted by varying the growth time, as maintaining the already low supersaturation was preferable. The goal was to grow the thinnest possible PL3 layer, as preliminary experiments indicated that this layer, being closest to the active EL layer, exhibited the highest emissions while absorbing most of the intensity of the primary emission. The thickness of the EL layer was gradually increased from S2 to S4 by increasing the growth time. This was necessary because the low transmittance measurements suggested that the initial thickness was insufficient. The EL and PL layers were separated by 1–2 μm thick n-type InP spacers to eliminate direct electronic coupling via charge carrier diffusion. From the empirical data, it was clear that there is an optimal layer thickness to all the films in the structure, which results in maximal emission intensities. Below and above the required thickness, the intensity decreases. The physical reason for this is explained later.

3.2. Morphological analysis

The layer thicknesses were measured by scanning electron microscopy (SEM), as shown in Fig. 3. The layer composition and the exact stoichiometry were validated by energy dispersive spectroscopy (EDS).

According to the SEM measurements, the layers thickness roughly corresponds to the intended, and the designed stoichiometry was confirmed. The grown layers are dense and smooth, the growth is continual from one layer to the next even at the transition between the 2 LPE steps. Their excellent crystallinity and epitaxy can clearly be seen from the images. The EDS measurements verified the composition of the layers, and the stoichiometry agreed well with the intended (in the range of EDS accuracy). From the measured thickness and composition values, the exact layer structure is shown in Fig. 3. While the composition of the layers can be reliably controlled and reproduced, precise control over layer thickness can be challenging. This is evident in the slight variations observed in the PL1 layer thickness between samples S1-S4, despite consistent preparation conditions. The thickness of the EL (1150 nm) layer was increased from 1.3 to 1.7 μm in samples S2-S4. The reduction of the most critical PL3 (1650 nm) layer thickness was achieved in the sample S3, while the thickness of PL3 (1500 nm) increased despite the intentions to keep it thin as well to reduce its high influence according to the PL measurements. (Growing InGaAsP layers with a bandgap around 1450 nm in LPE is challenging due to the material's tendency towards phase separation within the miscibility gap, making the precise control of composition and thickness difficult [18]).

3.3. Optical properties

Transmittance measurements (Fig. 5) are generally used to first evaluate the quality of the grown layers. The transmittance spectra clearly display the crystalline quality and the epitaxy of the layers, as well as the size of the bandgap. Therefore, the transmittance of the grown films was taken after the 1st and after the 2nd LPE growth steps as well. The active emitting layer and the one with the highest optical band gap in terms of wavelength were prepared in the 2nd step. Peaks in the derivative transmittance are indicators of the thickness and the band gap of the layers. Thinner anti-meltback layers are also detectable in the derivative transmittance spectra at wavelength 1150 nm and 1280 nm. (Note that beside the peaks belong to the grown layers, interference fringes are also visible on the derivative spectra).

Right after the first LPE growth process, photoluminescence spectra were measured. The PL 1320 nm and 1500 nm layers were grown in this step. It is clearly visible on the PL spectrum (Fig. 6) that PL emissions using excitation from the substrate side are different from the ones using excitation from the top side. The difference can be proved through simple optical model calculations, but for now, the following simplified explanation is sufficient:

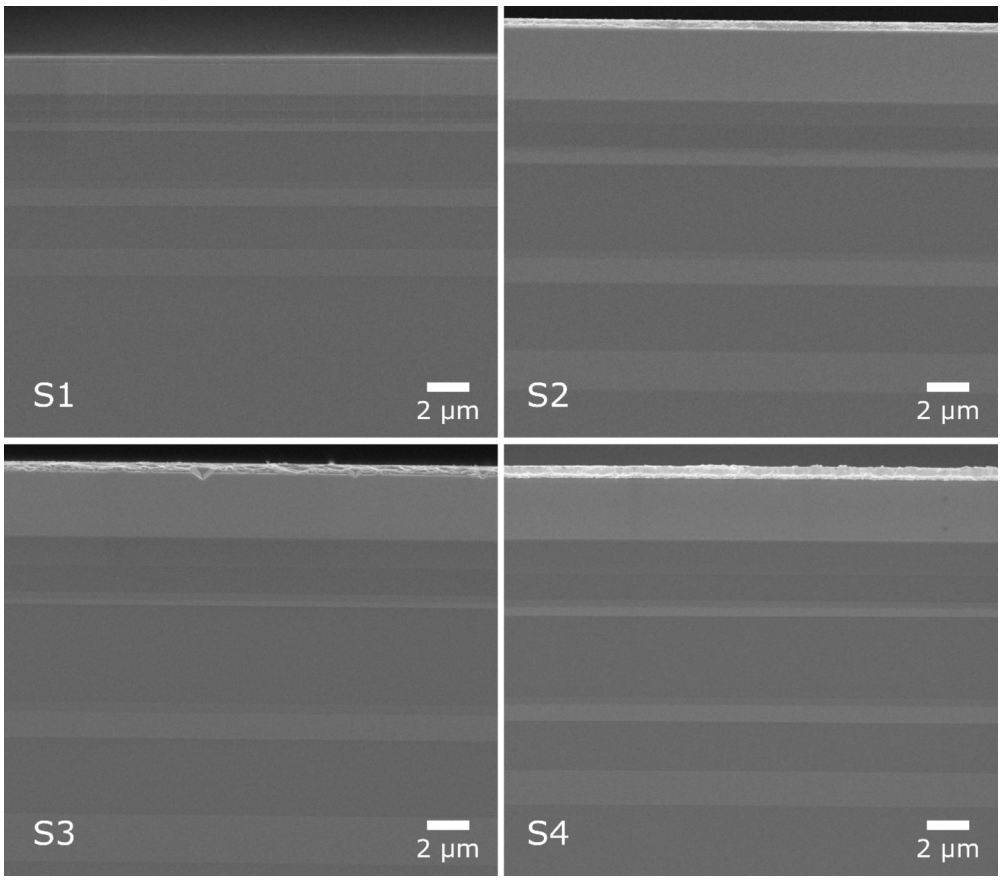

Fig. 3. The SEM images of the layer structures of the different LED structures. The growth direction is from bottom to top, the light path from top to bottom.

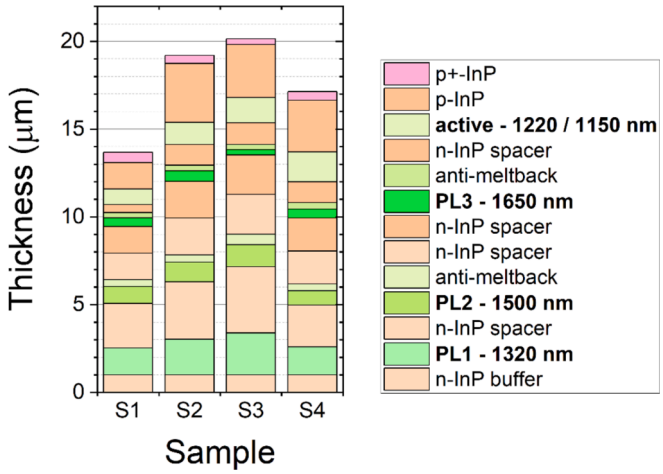

Fig. 4. The layer structures as measured by SEM, the substrate is at the bottom, followed by the buffer and then the layers.

a. excitation from top side: First, the excitation is partially absorbed in PL2–1500 nm (and in its anti-meltback) layer, then the secondary emitted 1500 nm passes through the sample uninterrupted. A part of the already weak leftover of the excitation is absorbed in PL2–1320 nm layer, and a 1320 nm wavelength is emitted here.
b. excitation from the bottom (substrate) side: First, the PL1–1320 nm layer absorbs the excitation partially and reemits a 1320 nm wavelength. The next PL2–1500 nm layer absorbs both the excitation and the 1320 nm wavelength partially, then reemits at 1500 nm wavelength.

In configuration (a.) – excitation from top side, the first PL layer dominates the whole PL spectrum. Even though this arrangement tends to simulate the normal operation of the device, further PL measurements were carried out in configuration b., excitation from the substrate side, to get evenly distributed PL emission spectra. The anti-meltback layers (1150 nm and 1280 nm) do not show up in the PL spectra, presumably due to the electrical coupling to the layer next to them, which have smaller bandgaps.

Fig. 7 shows normalized photoluminescent emissions at an excitation wavelength of 1070 nm. The graphs show the PL spectra recorded after the 1st LPE growth step (black curves) and right after the 2nd LPE growth step (red curves). The excitation was from the substrate side, where the layer order was the following:

- after LPE 1: PL1−1320 , PL2–1500 nm
- after LPE 2: PL1−1320 nm, PL2–1500 nm, PL3–1650 nm, the active layer–1220 nm or 1150 nm.

Right after the 1st LPE growth, only 2 PL layers are in the layer structure. Due to the low optical complexity of the layer structure, a clear inverse relationship can be observed between the layer thicknesses and the PL emissions in both PL1 and PL2 layers.

Measurements after LPE 2 show higher absorption at the excitation wavelength, and similar or lower emissions at peaks 1320 nm and 1500 nm, and reveal the layers grown in the 2nd LPE step. The PL emission of the active EL layers (S1: 1220 nm, S2-S4: 1150 nm) is barely detectable due to the high absorbance of the excitation wavelength on its way. Layer PL3 has also low emission, however it absorbs and reemits the previously generated secondary wavelengths as well. (The increased noise at the higher wavelength end of the spectrum is due to the correction of the signal in this low sensitivity range of the

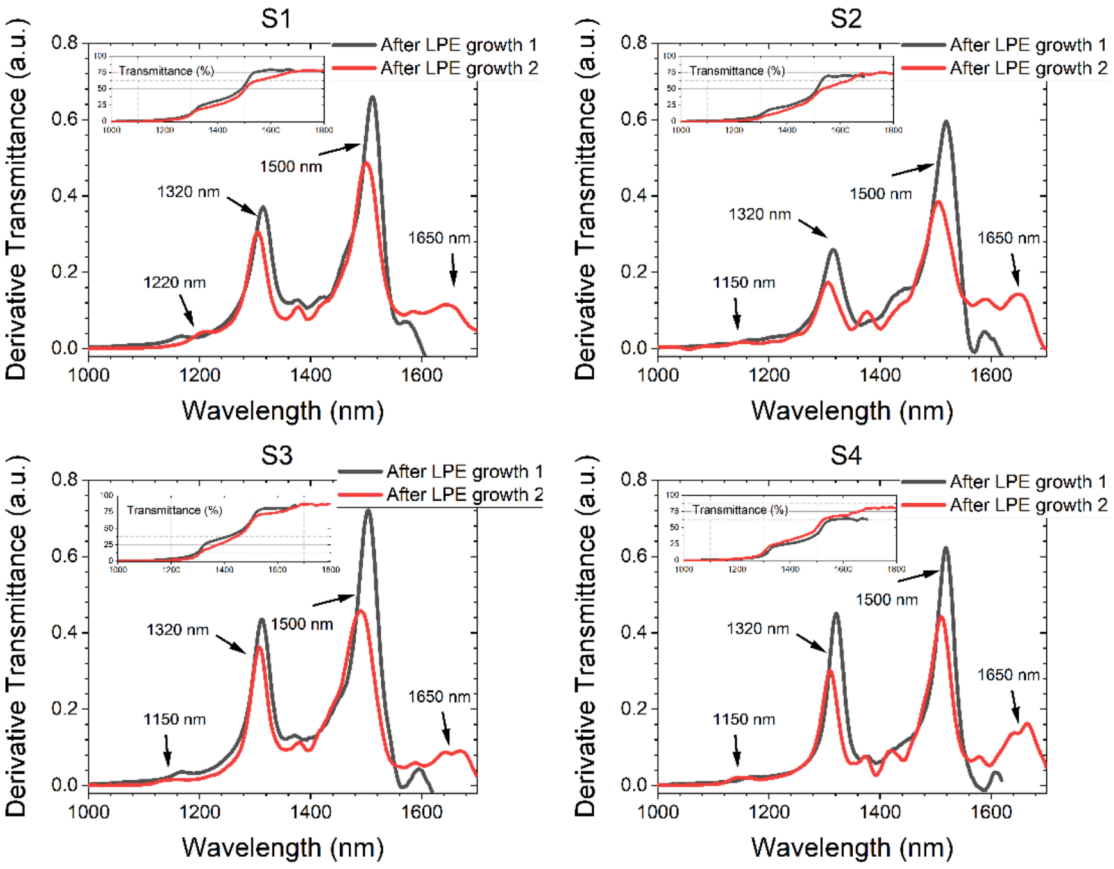

Fig. 5. The derivative transmittance spectra of the as grown layers.

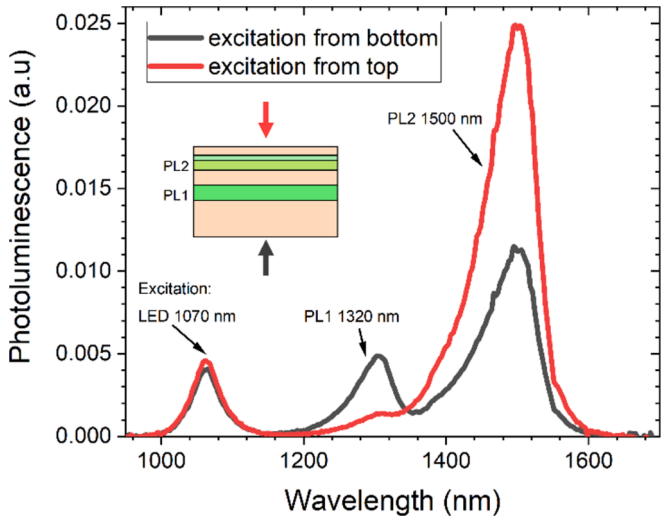

Fig. 6. PL spectrum of S1 using excitation wavelength 1070 nm from substrate (bottom) side and from top side.

spectrophotometer by scaling up).

3.4. Electroluminescence

After the layer growth steps, and the validation measurements, LED structures were fabricated by the procedure detailed in the experimental section. The wafers were diced, and the electroluminescence of the ready LED chips was measured.

Electroluminescence emissions were recorded with 10–100 mA forward current. The spectra (Fig. 8) show that the four deposition procedures resulted in different peak distributions. In the case of all four samples, the sum of the four peaks covers the wavelength region between 1100 to 1800 nm.

Optical power outputs (insets of Fig. 8) show saturation in this range of the forward current, where the active emitting layer structure (equivalent to our standard 1220 or 1150 nm LED) should have linear I-P characteristics. The stable energy distribution across the 1–100 mA forward current range suggests that the higher wavelength peaks are primarily due to optical coupling (photoluminescence) rather than direct radiative recombination within the PL layers. A previous study [21] using electron beam induced current measurements on a similar, but simpler LED layer structure confirmed that recombination primarily occurs within the p-i-n active region.

According to the measurements of S. Komiya et al. [22] emission intensities of PL layers should show a linear dependence on the intensity of the excitation source which was a Nd:YAG laser with a wavelength of 1064 nm and with a power output in the range of 10^{-1}-10^{4} W/cm^2 varied by neutral-density filters. In our case the PL measurements are carried out with a quite low, ca. 0.03 W/cm^2 excitation power, but in the case of the device tests, the internal optical power of the EL layer can be as high as 10^{2} W/cm^2 (@I_{fwd} = 100 mA). In any case, the PL emissions should be linearly coupled to the excitation. However, the emission peaks show a saturation tendency in the function of driving current in the range of 10–100 mA. The higher the wavelength of the peak, the sooner the saturation is reached. This also means that the distribution of the optical energy output spectrum shifts towards lower wavelengths with the driving current. Presumably, this is due to the increasing temperature caused by the driving current.

S. Komiya's other measurements showed that PL emission of layers tend to saturate with thickness above 1 μm, where the PL intensity was measured from the same side of the sample as the excitation. In the

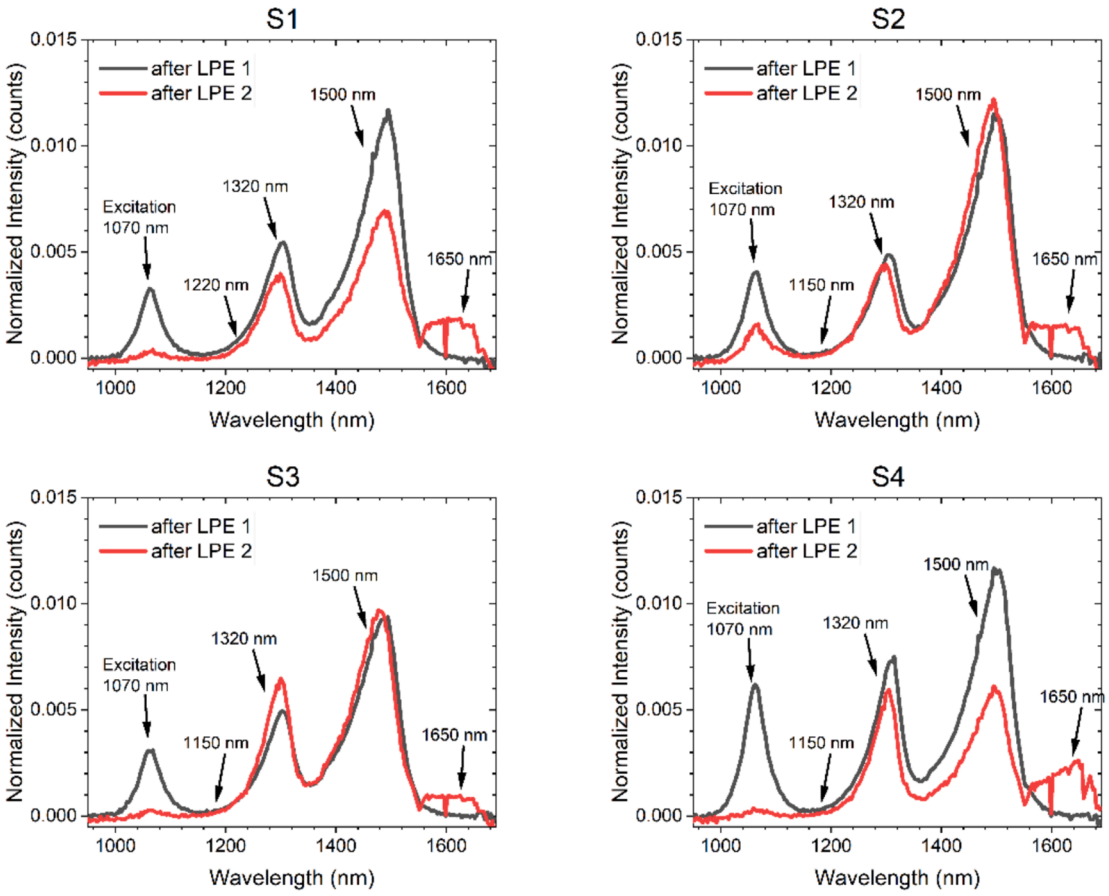

Fig. 7. Photoluminescence spectra of the grown layers.

present case, transmissive PL intensities were captured, which is why instead of a saturation trend, a maximum and then a fast decay of the PL intensities can be expected as a function of the thickness because of the self-absorption. In our case, it is hard to isolate the multiple coupled effects to attribute the peak intensity losses directly to the corresponding PL layer thicknesses. However, in general it can be said that the PL1 (1320 nm) layers with thickness 1530–2380 um show relatively weak intensities, while the PL3 (1650 nm) layers with thicknesses below 1 μm emit relatively high intensities in all 4 samples. In the case of PL3, the source of the excitation cannot only be the primary wavelength of the EL, but the secondary emissions of the other PL layers as well. Although S3 has the thinnest PL3 layer, its reduced absorption allows for increased excitation power to reach subsequent layers. This contributes to the highest summed output power and the most intense 1500 nm peak among the four samples.

3.5. Device performance

Sample S1 presents a good balance with the peaks covering the whole range. The high wavelength peaks are also dominant here, but the lower wavelength peaks are also apparent. Fig. 9 shows the distribution of the optical output power between the 4 emission peaks and the external quantum efficiency (EQE) as a function of forward driving current in the case of S1. The emission spectra were fitted with 4 peak functions. The asymmetric double sigmoidal (OriginLab Asym2Sig) function gave the best fit for both the photoluminescence and emission peaks in the wavelength domain, as suggested by refs. [23,24]. The offset parameter and the so called "FWHM" parameter of the Asym2Sig function were set and kept at 0. Because of the instability of the multi-peak fitting process, the amplitudes, centre wavelengths, the variances at low-energy side and the variances at high-energy side were kept in a reasonable range during the iteration process. The peak wavelengths, peak intensities, the real FWHM and peak areas (in energy domain as well) were calculated from the fitted parameters afterwards.

The optical energy distribution shows only 15 % variation in the forward current range of 1–100 mA. The EQE is 1.13 % at 50 mA, and the peak is 1.55 % at 19 mA which is ca. 242 A/cm^2 considering the geometry of the fabricated LEDs. These values are somewhat lower than the EQE of the standard InGaAsP/InP based DHJ LEDs, which is typical 1.9–2.5 % at the 50 mA (637 A/cm^2) in continuous mode [25]. The power loss due to the conversion was calculated in the case of S1 assuming that all 3 secondary wavelength emissions derived from the 3 PL layers excited by the primary wavelength alone. Assuming that the internal photon to photon conversion efficiency in the PL layers are 100 %, then the photon energy to photon energy conversion efficiency is $\lambda_{exc}/\lambda_{PL}$ and the optical power of the PL emission is the following: $P_{\lambda_{PL}} = P_{\lambda_{exc}} \frac{\lambda_{exc}}{\lambda_{PL}}$.

The total optical power output of S1 at a continuous 50 mA forward current is 0.46 mW, and the EQE is 1.13 %. The output power distribution was calculated based on the fitted emission peaks at a 50 mA driving current. The optical power of the excitation in every PL layer was calculated using the photon energy conversion efficiency formula for all four peaks (see Table 2).

After summing up the excitation power of every PL layers, the approximated total amount of optical power absorbed by the PL layers should be at least 0.582 mW at wavelength 1220 nm (including the transmitted part of the primary emission). The emitted power of the active layer was estimated from the transmittance of the LED wafer and this transmitted part of the primary emission. The transmittance at the active wavelength is around 3–4 %, therefore the estimated optical power generated by electroluminescence is 0.88–1.12 mW, and the overall power loss could be 34–48 %.

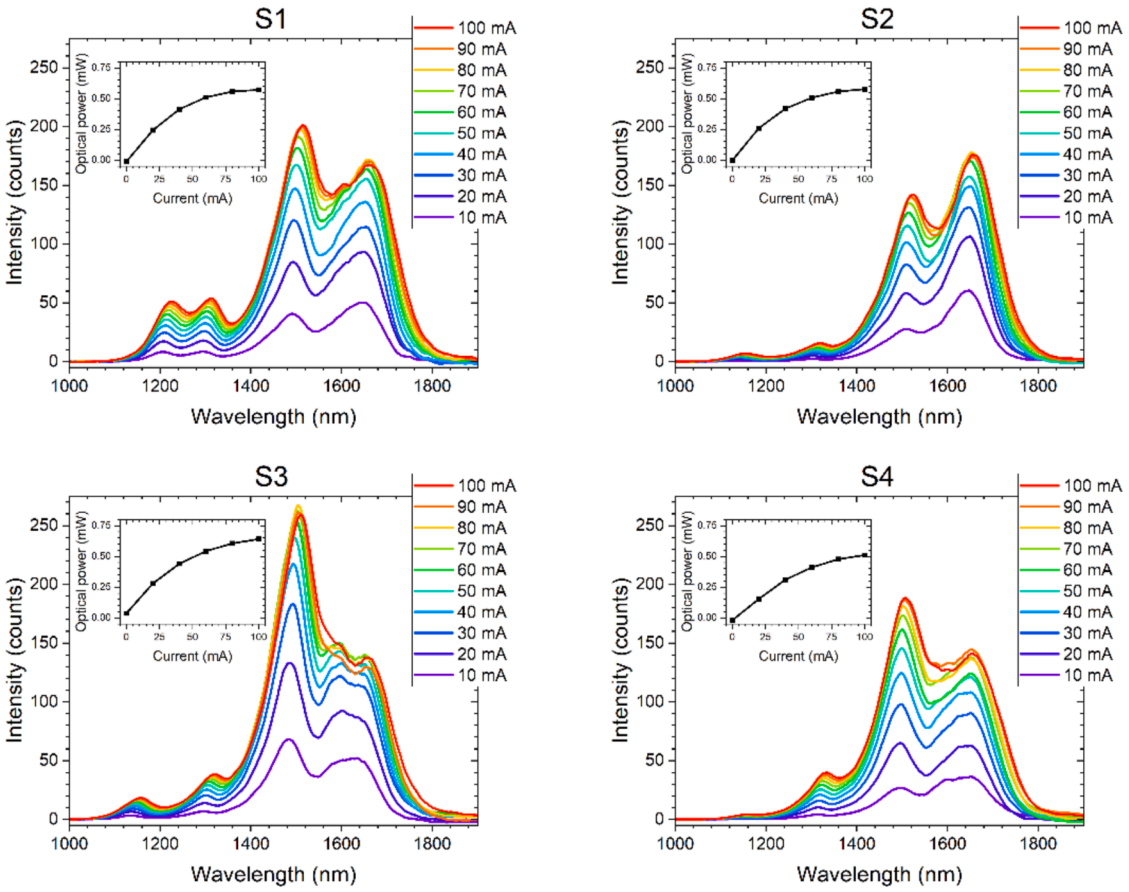

Fig. 8. Emission spectra of the fabricated multi-wavelength LEDs at driving current 10–100 mA. The insets show the corresponding optical power over the whole wavelength range vs. forward current.

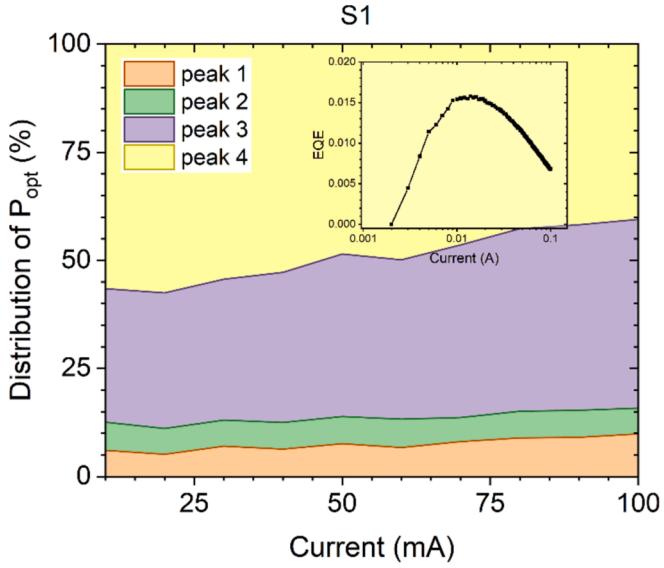

Fig. 9. The distribution of the output optical power between the emission peaks as a function of forward current. Inset shows the EQE measured at room temperature as a function of forward current.

Presumably the optical power is lost mainly due to the unwanted self-absorption of the too thick PL layers mentioned earlier. Besides, the 1.32 V voltage value at 50 mA current is somewhat high at this DHJ configuration, which refers to a moderate series resistance in the current path and also lowers the efficiency. Due to the limitation in the number of layers that can be grown in the LPE system, the layer structure deviates from the already optimized single emission wavelength LED structure, which results in the unideal performances. The EQE values of the samples S1, S2, S3 and S4 at 50 mA were 1.13 %, 1.17 %, 1.38 %, and 0.9 % respectively, and the power losses were 34–48 %, 46–78 %, 48–71 % and 32–57 % respectively.

4. Conclusions

The present work explores the possibilities of preparing broad band NIR LEDs without the use of phosphorus materials. In a sequential LPE growth process an electroluminescent LED layer structure is covered with three photoluminescent layers, which absorb a portion of the primary light and reemit at different wavelengths. The resulting spectrum is a sum of four emission peaks, which can be designed and controlled through the thickness and the band gap (stoichiometry) of the layers. As all the layers can be grown epitaxially in one growth step, the resulting devices have high efficiency and excellent spectral qualities. The method is straightforward, low-cost and very applicable. The thus prepared NIR LEDs with broad emission spectrum have the potential to be used in a wide range of applications, such as medical imaging and spectroscopy.

Presently, estimating the electroluminescent emission from the TD or PL measurements is difficult. The exact roles of the PL layers in the emission intensity distribution and the optimal multilayer structure should be numerically calculated based on multiple internal reflectance, absorbance and photoluminescent efficiency. This could be the scope of future work.

CRediT authorship contribution statement

Zoltán Szabó: Writing – original draft, Validation, Methodology, Investigation. **Barbara Beiler:** Writing – review & editing, Methodology. **Zsófia Baji:** Writing – review & editing.

Declaration of competing interest

The authors declare that they have no known competing financial interests or personal relationships that could have appeared to influence the work reported in this paper.

Acknowledgments

This work is partially supported by the Chips Joint Undertaking and the National Research, Development and Innovation Fund (NKFIA) via UNLOOC (Grant No. 101140192) and TKP INBIOM (Grant No. TKP2021-EGA-04) projects.

I would like to express my sincere gratitude to Vilmos Rakovics for introducing me to this research field and generously sharing his expertise.

Appendix A. Supplementary data

Supplementary materials provide detailed experimental data, including layer structure parameters, optical spectra, and electrical characteristics, to support the findings presented in the main text. Supplementary data to this article can be found online at https://doi.org/10.1016/j.jcrysgro.2024.128045.

Data availability

Data will be made available on request.

References

[1] C. Pasquini, Near Infrared Spectroscopy: fundamentals, practical aspects and analytical applications, J. Braz. Chem. Soc. 14 (2) (2003) 198–219, https://doi.org/10.1590/S0103-50532003000200006.

[2] M. Mesic, V. Corluka, and Z. Valter, "Analysis of some parameters influencing moisture quantity measurements in wheat with NIR technique," *2005 18th International Conference on Applied Electromagnetics and Communications, ICECom 2005*, 2005, doi: 10.1109/ICECOM.2005.204959.

[3] R. J. A. Do Nascimento, G. R. De MacEdo, E. S. Dos Santos, and J. A. De Oliveira, "Real time and in situ Near-Infrared Spectroscopy (Nirs) for Quantitative Monitoring of Biomass, Glucose, Ethanol and Glycerine concentrations in an alcoholic fermentation," *Brazilian Journal of Chemical Engineering*, vol. 34, no. 2, pp. 459–468, Apr. 2017, doi: 10.1590/0104-6632.20170342S20150347.

[4] R. Risoluti, G. Gullifa, S. Materazi, Assessing the quality of milk using a multicomponent analytical platform microNIR/chemometric, Front. Chem. 8 (Dec. 2020) 614718, https://doi.org/10.3389/FCHEM.2020.614718/BIBTEX.

[5] U. Bassey, et al., The potential of NIR spectroscopy in the separation of plastics for pyrolysis, Electronic Imaging 33 (3) (Jun. 2021) 1–14, https://doi.org/10.2352/ISSN.2470-1173.2021.3.MOBMU-143.

[6] I. O. Afara, I. Prasadam, Z. Arabshahi, Y. Xiao, and A. Oloyede, "Monitoring osteoarthritis progression using near infrared (NIR) spectroscopy OPEN", doi: 10.1038/s41598-017-11844-3.

[7] L. Zhang, et al., A high efficiency broad-band near-infrared Ca2LuZr2Al3O12:Cr3+ garnet phosphor for blue LED chips, J. Mater Chem. C Mater 6 (18) (May 2018) 4967–4976, https://doi.org/10.1039/C8TC01216D.

[8] X. Ding, Q. Zhang, Multi spectral responsive near infrared-II broad emission material and its LED device and imaging research, Ceram. Int. 47 (24) (Dec. 2021) 34851–34859, https://doi.org/10.1016/J.CERAMINT.2021.09.026.

[9] V. Rajendran, et al., Super broadband near-infrared phosphors with high radiant flux as future light sources for spectroscopy applications, ACS Energy Lett. 3 (11) (Nov. 2018) 2679–2684, https://doi.org/10.1021/ACSENERGYLETT.8B01643/SUPPL_FILE/NZ8B01643_SI_001.PDF.

[10] D. Dai, et al., Broad band emission near-infrared material Mg3Ga2GeO8:Cr3+: Substitution of Ga-In, structural modification, luminescence property and application for high efficiency LED, J. Alloy. Compd. 806 (Oct. 2019) 926–938, https://doi.org/10.1016/J.JALLCOM.2019.07.166.

[11] J.W. Shi, T.J. Hung, Y.Y. Chen, Y.S. Wu, W. Lin, Y.J. Yang, InP-based transverse junction light-emitting diodes for white-light generation at infrared wavelengths, IEEE Photon. Technol. Lett. 18 (19) (Oct. 2006) 2053–2055, https://doi.org/10.1109/LPT.2006.883296.

[12] T.P. Lee, C.A. Burrus, A.G. Dentai, Dual wavelength surface emitting InGaAsP l.e.d. s, Electron. Lett 16 (22) (Oct. 1980) 845–846, https://doi.org/10.1049/EL:19800600.

[13] V.V. Volkov, et al., LPE growth and characterization of InGaAsP/InP heterostructures: IR light-emitting diodes at 1.66 μm. Application to the remote monitoring of methane gas, Sens Actuators A Phys. 62 (1–3) (Jul. 1997) 624–632, https://doi.org/10.1016/S0924-4247(97)01377-0.

[14] V. Rakovics, J. Nádas, I. Réti, C.S. Dücső, G. Battistig, "Growth and characterization of broad spectrum infrared emitting GaInAsP/InP heterostructures", J. Cryst. Growth 468 (2017) 572–575, https://doi.org/10.1016/J.JCRYSGRO.2016.11.123.

[15] T.P. Lee, A.G. Dentai, Power and modulation bandwidth of GaAs–AlGaAs high-radiance LED's for optical communication systems, IEEE J. Quantum Electron. 14 (3) (1978) 150–159, https://doi.org/10.1109/JQE.1978.1069761.

[16] M.A. Digiuseppe, H. Temkin, W.A. Bonner, Large area LPE growth of InGaAsP/InP double heterostructures on InP preserved in a phosphorus ambient, J. Cryst. Growth 58 (1) (Jun. 1982) 279–284, https://doi.org/10.1016/0022-0248(82)90237-8.

[17] P. P. Deimel, "Calculations for integral lenses on surface-emitting diodes," *Applied Optics, Vol. 24, Issue 3, pp. 343-348*, vol. 24, no. 3, pp. 343–348, Feb. 1985, doi: 10.1364/AO.24.000343.

[18] E. Kuphal, Phase diagrams of InGaAsP, InGaAs and InP lattice-matched to (100) InP, J. Cryst. Growth 67 (3) (1984) 441–457, https://doi.org/10.1016/0022-0248(84)90036-8.

[19] O. Wada, S. Yamakoshi, M. Abe, Y. Nishitani, T. Sakurai, High radiance InGaAsP/InP lensed LED's for optical communication systems at 1.2-1.3 μm, IEEE J. Quantum Electron. 17 (2) (1981) 174–178, https://doi.org/10.1109/JQE.1981.1071054.

[20] J. I. Pankove, "Optical process in semiconductors," *Dover Publications, Inc.*, vol. 119, no. 5, p. 450, 1975.

[21] V. Rakovics, J. Nádas, I. Réti, C. Dücső, G. Battistig, Growth and characterization of broad spectrum infrared emitting GaInAsP/InP heterostructures, J. Cryst. Growth 468 (Jun. 2017) 572–575, https://doi.org/10.1016/J.JCRYSGRO.2016.11.123.

[22] S. Komiya, A. Yamaguchi, I. Umebu, T. Kotani, Studies of Photoluminescence Intensity in The Inp/Ingaasp/Inp Double Heterostructure, Jpn. J. Appl. Phys. 23 (3) (Mar. 1984) 308–311, https://doi.org/10.1143/JJAP.23.308/XML.

[23] F. Reifegerste, J. Lienig, Modelling of the temperature and current dependence of LED spectra, J. Light Visual Environ. 32 (3) (Aug. 2008) 288–294, https://doi.org/10.2150/JLVE.32.288.

[24] R. Supronowicz and I. Fryc, "The LED spectral power distribution modelLED by different functions-how spectral matching quality affected computed LED color parameters," *2019 2nd Balkan Junior Conference on Lighting, Balkan Light Junior 2019 - Proceedings*, Sep. 2019, doi: 10.1109/BLJ.2019.8883564.

[25] V. Rakovics, A.N. Imenkov, V.V. Sherstnev, O.Y. Serebrennikova, N.D. Il'inskaya, Y.P. Yakovlev, High-power LEDs based on InGaAsP/InP heterostructures, Semiconductors 48 (12) (2014) 1653–1656, https://doi.org/10.1134/S1063782614120173.